Topological order in densely packed anisotropic colloids

William Zygmunt, Erin G. Teich, Greg van Anders, and Sharon C. Glotzer

Phys. Rev. E **100**, 032608 — Published 25 September 2019

DOI: 10.1103/PhysRevE.100.032608

Topological Order in Densely Packed Anisotropic Colloids

William Zygmunt,[1] Erin G. Teich,[2,*] Greg van Anders,[1,2,3,†] and Sharon C. Glotzer[1,2,3,4]
[1]*Department of Chemical Engineering, The University of Michigan, Ann Arbor, MI 48109-2136, USA*
[2]*Applied Physics, The University of Michigan, Ann Arbor, MI 48109-1040, USA*
[3]*Department of Physics, The University of Michigan, Ann Arbor, MI 48109-1040, USA*
[4]*Department of Materials Science and Engineering, University of Michigan, Ann Arbor, MI 48109-2136, USA*

The existence of topological order is frequently associated with strongly coupled quantum matter. Here, we demonstrate the existence of topological phases in classical systems of densely packed, hard, anisotropic polyhedrally shaped colloidal particles. We show that previously reported transitions in dense packings lead to the existence of topologically ordered thermodynamic phases, which we show are stable away from the dense packing limit. Our work expands the library of known topological phases, whose experimental realization could provide new means for constructing plasmonic materials that are robust in the presence of fluctuations.

I. INTRODUCTION

Topological phases are exotic states of matter that are typically associated with strongly interacting quantum systems, in which topological protection stabilizes certain physical behaviors against environmental perturbations [1]. In quantum systems, protection of this type can be invaluable in applications for which coherence is crucial. In a similar spirit, many applications for classical soft matter systems of colloidal nanoparticles would benefit from topological order in the presence of environmental perturbations. In colloidal systems, entropic effects are important [2–4] and typical interaction strengths are on the order of the thermal scale. Indeed, recent work has shown that thermal fluctuations in soft systems can, in a variety of contexts, drive structural reconfiguration [5–8], an important feature of functional nanomaterials. However, for other applications, the preservation of structural order against thermal fluctuations is vital. If soft matter was topologically ordered, it could be used in building structures with robust features.

Recent work [9] has shown that topological states can exist in specialized classical mechanical systems, and that the dynamics of classical systems can manifest topological effects [10, 11]. The topological states that occur in those systems are expressed in terms of Witten indices, whose existence relies on the spectrum of excitations in nearly-isostatic lattices. Additionally, topologically protected phases exist in a variety of classic phononic [12–17] and photonic [18] systems.

Here, we show that the point-set topology of contacts that distinguishes structures of hard colloids at infinite pressure (aka "putative densest packings") [19] leads to the existence of topologically distinct phases. We prove peturbatively that, in general, topologically distinct putative densest packings lead to the existence of associated thermodynamic phases away from infinite pressure. We demonstrate numerically that topological order persists at finite pressure. Surprisingly, we find that thermodynamic phases that are topologically protected at the highest possible packing densities preserve near-perfect topological order at packing densities sufficiently low that topological protection need not persist.

Our approach provides a general framework for investigating and classifying the structure of thermodynamic systems of hard colloids near the dense packing limit. The topological order we observe is of a strikingly different origin – and consequently, has different properties – than topological states in quantum matter. Ref. [9] showed that the existence of topological phases is not uniquely the preserve of strongly interacting quantum matter, and our results raise the possibility that topological order is a widespread phenomenon in classical systems.

II. ANALYTICAL FIRST-ORDER PHASE TRANSITION AT INFINITE PRESSURE

Ref. [19] showed that, for families of hard anisotropic shapes at infinite pressure, continuous deformations of particle shape result in continuous changes in putative densest packings. It was also shown that non-analytic behavior in curves, surfaces, or hypersurfaces $\phi_d(\alpha_i)$ of maximal packing density ϕ_d as a function of particle shape α_i occur if and only if there is a change in the point-set topology of contacts between particles in the dense packing structure; Fig. 1 illustrates this point. We argue that, generically, this leads to distinct, solid thermodynamic phases away from infinite pressure. Since pressure is defined in units of k_BT, we can think of the infinite pressure limit as a sort of zero temperature limit of the system, which may be a more useful way to think about these hard particle systems in reference to other works involving topological order. Note that the focus of this analysis is to draw a distinction between adjacent solid phases, rather than on the existence of distinct solid and liquid phases.

We make our argument using the framework of digital alchemy [20]. Digital alchemy extends the traditional thermodynamic ensemble for particle self-assembly through consideration of thermodynamically conjugate variables (termed "alchemical potentials" μ) coupled to changes in particle attributes. Here, we consider changes in particle shape as the alchemical variable for the packings in [19] and the associ-

---

[*] Current Address: Department of Bioengineering, University of Pennsylvania, Philadelphia, PA, 19104, USA
[†] Current Address: Department of Physics, Engineering Physics, and Astronomy, Queen's University, Kingston, ON, K7L 3N6, Canada, gva@queensu.ca

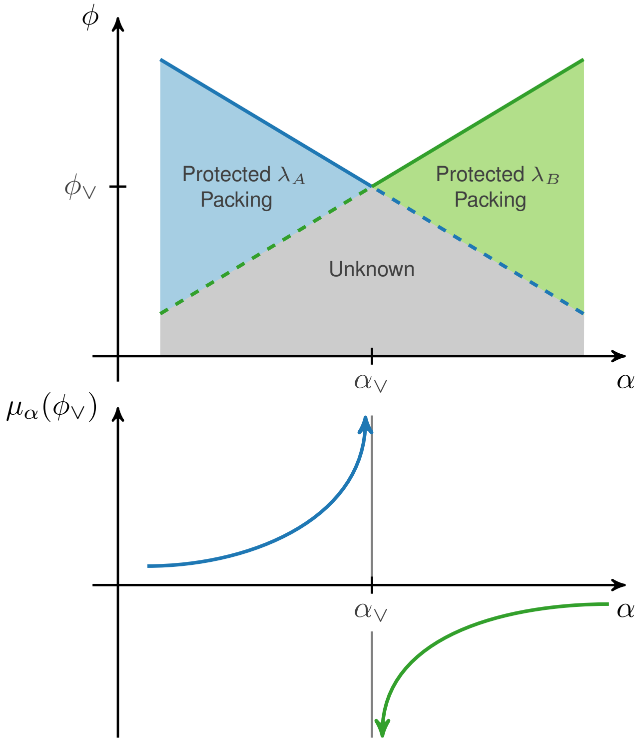

FIG. 1. Surfaces (solid blue and green lines) of maximal packing density (ϕ_d) as a function of particle shape (α) have been shown [19], in general, to exhibit non-analytic behavior at the point $(\alpha_\vee, \phi_\vee)$ that is associated with a change in the topology of contacts between adjacent particles. Within the blue and green triangular regions, dense packings exhibit topological distinction by particle contacts. However, within the gray region bounded above by the dashed blue and green lines, it is unknown, in general, whether topological contact types persist (top panel). We show that there is a first-order phase transition, indicated by the divergence of the so-called alchemical potential [20] near the valley packing discontinuity (bottom panel).

ated alchemical potential is given by

$$\mu_\alpha = \frac{1}{N}\frac{\partial F}{\partial \alpha}\ , \tag{1}$$

where N is the number of particles in the system, F is the free energy, and α is a shape parameter. To understand the phase behavior of dense suspensions of anisotropic colloids away from infinite pressure, it is convenient to study the alchemical potential in the vicinity of the intersection of two packing curves, where there is a change in the topology of particle contacts ($\alpha_\vee, \phi_\vee$ in Fig. 1).

It was previously shown [19] that for generic, anisotropic colloids, each fragment of the dense packing surface is a topologically distinct packing. We will assert that in each topological equivalence class of packings there are the same number of "microstates" or entropy. This is a reasonable assumption because in most cases there is only one topologically allowed dense packing, and in the cases where there are sliding surfaces, the sliding surfaces should be topologically equivalent. We assume that, for some shape with alchemical parameter α describing the particle shape, there is a densest packing ϕ_d. We can find the free energy at a lower packing density ϕ via thermodynamic integration according to

$$F(\phi,\alpha) = F(\phi_d(\alpha),\alpha) - \int_\phi^{\phi_d} d\phi' \frac{\partial F(\phi',\alpha)}{\partial \phi'}. \tag{2}$$

Using the relationship between packing density and volume, and the definition of pressure, this can be written as

$$F(\phi,\alpha) = F(\phi_d(\alpha),\alpha) - \int_\phi^{\phi_d} d\phi' \frac{N\ell^d P(\phi')}{\phi'^2}, \tag{3}$$

where ℓ is a characteristic length scale for the system, which we take to be the particle size, and assume that changes in α preserve the particle volume. For convenience, we will take $P^* = \ell^d \beta P$ to be the dimensionless pressure (where β is inverse temperature).We decompose the free energy into the kinetic part and the configurational part. We assume that the configurational part $\tilde{F}(\phi_d(\alpha),\alpha)$ is constant along a single topological family of packings, and the kinetic part F_k does not depend on density, so that

$$F(\phi,\alpha) = F_k(\alpha) + \tilde{F}(\phi_\vee,\alpha_\vee) - \int_\phi^{\phi_d} d\phi' \frac{NP^*(\phi')}{\beta\phi'^2}, \tag{4}$$

where we are following the notation of [20] for decomposing the free energy into kinetic and configurational parts [21]. Take $\Delta\alpha$ as the range over which the packing is optimal, and also take $\delta\alpha$ so that

$$0 < \delta\alpha \ll \Delta\alpha. \tag{5}$$

We then approximate $F(\phi_\vee, \alpha_\vee - \delta\alpha)$ using the midpoint rule as

$$F(\phi_\vee,\alpha_\vee-\delta\alpha) \approx F_k(\alpha_\vee-\delta\alpha) + \tilde{F}(\phi_\vee,\alpha_\vee) - \frac{N(\phi_d-\phi_\vee)}{2\beta}\left(\frac{P^*(\phi_d)}{\phi_d^2} + \frac{P^*(\phi_\vee)}{\phi_\vee^2}\right) \tag{6}$$

where ϕ_d is evaluated at $\alpha_\vee - \delta\alpha$. We can approximate

$$\phi_d(\alpha_\vee-\delta\alpha) - \phi_\vee \approx \delta\alpha \left|\frac{\partial\phi_d}{\partial\alpha}\right|_{\alpha=\alpha_\vee} \tag{7}$$

so that

$$\begin{aligned} F(\phi_\vee,\alpha_\vee-\delta\alpha) \approx{}& F_k(\alpha_\vee-\delta\alpha) + \tilde{F}(\phi_\vee,\alpha_\vee) \\ &- \frac{N\delta\alpha}{2\beta}\left|\frac{\partial\phi_d}{\partial\alpha}\right|_{\alpha=\alpha_\vee}\left(\frac{P^*(\phi_d)}{\phi_d^2} + \frac{P^*(\phi_\vee)}{\phi_\vee^2}\right). \end{aligned} \tag{8}$$

We can estimate the alchemical potential in the limit that α approaches $\alpha_\vee$ from the left as

$$\mu_\alpha \approx \frac{1}{N\delta\alpha}\Big(F_k(\alpha_\vee) - F_k(\alpha_\vee - \delta\alpha) + \frac{N\delta\alpha}{2\beta}\left|\frac{\partial\phi_d}{\partial\alpha}\right|_{\alpha=\alpha_\vee}\left(\frac{P^*(\phi_d)}{\phi_d^2} + \frac{P^*(\phi_\vee)}{\phi_\vee^2}\right)\Big) \tag{9}$$

so that

$$\mu_\alpha \approx \frac{1}{N}F_k'(\alpha_\vee) + \frac{1}{2\beta}\left|\frac{\partial\phi_d}{\partial\alpha}\right|_{\alpha=\alpha_\vee}\left(\frac{P^*(\phi_d)}{\phi_d^2} + \frac{P^*(\phi_\vee)}{\phi_\vee^2}\right). \tag{10}$$

The first term in Eq. (10) is a correction factor that comes from differentiating the trace of the moment of inertia tensor. As long as the shape parametrization is continuous, this term is finite and in [19] it certainly always is. However, $P^*(\phi_d)$ is formally infinite. That means $\mu_\alpha \to \infty$ as $\alpha \to \alpha_\vee^-$. If we carry out the same consideration for $\alpha_\vee + \delta\alpha$ everything carries through up to Eq. (10), except that the sign of the second term is reversed. This means $\mu_\alpha \to -\infty$ as $\alpha \to \alpha_\vee^+$. A sketch of this result is in Fig. 1.

μ_α is a first derivative of the free energy, which means that $\phi_\vee, \alpha_\vee$ is a first order thermodynamic phase transition. Another way of seeing this is the fact that the alchemical potential diverges near $\alpha_\vee$, meaning that at $\phi_\vee$ for any finite alchemical potential the system will have a thermodynamically preferred α that is a finite distance from $\alpha_\vee$. This means that if we regard α as an order parameter, there is no way at $\phi_\vee$ of having it take the value of $\alpha_\vee$, so that it must change discontinuously. We note that μ_α can also be interpreted as a stress that results from a strain $d\alpha$ [20]. This transition exists solely because of the non-analytic behavior of the dense packing surface, which reflects the topology of contacts among densely packed particles.

III. DELINEATION OF TOPOLOGICAL PHASES

Next we consider what happens below maximum packing density. We consider packings λ_i where $i \in \{A, B\}$; λ_A and λ_B are on either side of the phase transition shown schematically in Fig. 1. To distinguish between these packings, we construct an order parameter that takes advantage of the way λ_A and λ_B are defined topologically. Ref. [19] defines each packing according to the types of contacts (face-face, face-vertex, face-edge, vertex-vertex, vertex-edge and edge-edge) shared between adjacent particles. These contacts map to a set of intersection equations that mathematically describe each contact by relating particle shape parameters to the geometry of the two particle unit cell of the packing, described by vectors for the lattice and particle(s) within the unit cell. Each packing λ_i has K_i unique (meaning unshared with the other packing) intersection inequalities $\left|C_{i,k}\right| \geq 0$ (where $k = 1, 2, \ldots, K_i$) that define the packing. As an example, a packing λ_A might be described by a relation $C_{A,1} = [a\cdot < -1, 1, 1 > -(\alpha_a + \alpha_c)]$, where a is a lattice vector and α_a and α_c are parameters that describe particle shape. Note that the range of parameters could include any lattice vector (a, b, c), the displacement vector between the two particles in the unit cell (d), or any of three shape parameters (α_a, α_b, α_c). Three shape parameters fully characterize the family of particle shapes [19] considered in this paper; we describe them fully in the next section.

When the shape parameters and unit cell geometry correspond to densest packing, all the $C_{i,k} = 0$. If the geometry of the unit cell does not correspond to the densest packing, then some $\left|C_{i,k}\right| \geq 0$. Changes in unit cell geometry (while particle shape is fixed) effectively provide a means of measuring changes to particle contact; at lower packing densities, then, the saturation or near-saturation of the intersection inequalities (i.e. all $C_{i,k} \approx 0$) would imply that particle contacts have (through thermal fluctuation) remained approximately equal to the particle contacts at infinite pressure, preserving unit cell geometry and topological order.

We now define an order parameter of the form θ_{ij} where i represents a stable or metastable thermodynamic phase that is putatively isostructural with λ_i [22] and λ_j is the packing against which the state will be evaluated. For example, θ_{AA} is defined as the evaluation of a packing λ_A in its own intersection equations (those of λ_A), and it evaluates to unity at maximal packing density by construction. Conversely, θ_{AB} (pertaining to the same packing λ_A evaluated in the intersection equations of λ_B) evaluates to zero at maximal packing by construction.

To construct θ_{ij}, several variables must first be defined. The packing λ_i is a function of particle shape α and packing density $\phi \leq \phi_d$ by definition. We define ξ_{ij} (a function of particle shape α and packing density ϕ) to reflect the evaluation of packing λ_i in the intersection equations of packing type λ_j as

$$\xi_{ij}(\phi, \alpha) = e^{-\frac{1}{K_j}\sum_{k=1}^{K_j}\left|C_{j,k}(\lambda_i(\phi,\alpha))\right|}. \tag{11}$$

When $\phi = \phi_d$, ξ_{ij} describes the saturation of λ_j's intersection equations by λ_i at its maximum packing density, lying on its putative densest packing surface. We thus denote this special case by

$$\xi_{ij}^{\text{ideal}} = \xi_{ij}(\phi_d, \alpha). \tag{12}$$

To construct a generalized order parameter for a set of two adjacent packings λ_A and λ_B, we then compute four quantities ($\xi_{AA}, \xi_{AB}, \xi_{BA}, \xi_{BB}$) that consider all four evaluation types in $i \in \{A, B\}$ and $j \in \{A, B\}$, which we use to build vectors that represent coordinates in the $[\xi_{iA}, \xi_{iB}]$ plane

$$\mathbf{D_A} = \Big[\xi_{AA}, \xi_{AB}\Big] \ , \ \mathbf{D_B} = \Big[\xi_{BA}, \xi_{BB}\Big]. \tag{13}$$

Similarly, we construct vectors to represent the maximum density packings

$$\mathbf{D}_{\mathbf{A}}^{\mathbf{ideal}} = \Big[\xi_{AA}^{\text{ideal}}, \xi_{AB}^{\text{ideal}}\Big] \ , \ \mathbf{D}_{\mathbf{B}}^{\mathbf{ideal}} = \Big[\xi_{BA}^{\text{ideal}}, \xi_{BB}^{\text{ideal}}\Big]. \tag{14}$$

The distance between the ideal structures in the $[\xi_{iA}, \xi_{iB}]$ plane is

$$\mathbf{D}_{\mathbf{AB}}^{\mathbf{ideal}} = \sqrt{(\mathbf{D}_{\mathbf{A}}^{\mathbf{ideal}} - \mathbf{D}_{\mathbf{B}}^{\mathbf{ideal}}) \cdot (\mathbf{D}_{\mathbf{A}}^{\mathbf{ideal}} - \mathbf{D}_{\mathbf{B}}^{\mathbf{ideal}})}. \tag{15}$$

Finally, we define θ_{ij} to distinguish the topology of the two packings, making a generalized expression for any packing λ_i evaluated in the intersection equations of a packing type λ_j

$$\theta_{ij} = 1 - \frac{\sqrt{(\mathbf{D}_{\mathbf{i}} - \mathbf{D}_{\mathbf{j}}^{\mathbf{ideal}}) \cdot (\mathbf{D}_{\mathbf{i}} - \mathbf{D}_{\mathbf{j}}^{\mathbf{ideal}})}}{\mathbf{D}_{\mathbf{AB}}^{\mathbf{ideal}}}. \tag{16}$$

Since we do not have a method to directly measure the topological invariant of a packing, we use our order parameter to estimate topological order of a packing λ_i being evaluated using the intersection equations of a packing type λ_j. We find that our order parameter, in some specific packings, can tend to underreport topological order by a small amount (see Section VB) but visual inspection confirms that the same contacts still manifest themselves in these packings. Since we are trying to show the mere existence of topological order in these systems, a slight underreport does not affect our overall conclusions.

IV. NUMERICAL METHODS

Topologically distinct packings can be found for a range of families of anisotropic colloids. For concreteness, we considered packings in the two-parameter family of triangle invariant polyhedral shapes, Δ_{323}, reported in Ref. [19]. This family of shapes includes three Platonic solids (tetrahedron, octahedron, cube) and truncations thereof. The family can be described by two independent shape parameters, α_a and α_c (following the convention of [8]), denoting shape edge truncation and vertex truncation respectively. In [19], these variables are instead called u and v respectively. A third shape parameter that appears in the intersection equations, α_b, is equal to 1 in this shape family. Authors in [19] showed the existence of 75 topologically distinct two-particle dense packings of polyhedra in this family. This family has the largest number of closely spaced packings, which one might expect could reduce stability, making this set of systems a suitable candidate for investigating stability. Also, because the number of adjacent packing states is too large to study exhaustively, we arbitrarily chose two for extensive study. We chose two distinct packing boundaries (valleys which have a packing λ_i on either side, where $i \in \{A, B\}$), with one boundary (I) located between phases labelled ‘52’ and ‘58’ and the other boundary (II) between phases labelled ‘74’ and ‘69’ (numbering convention can be found in Ref. [19]).

For each boundary, we chose one shape parameter (either α_a or α_c) to remain constant, and then moved along the axis of the other α. For boundary I, we studied a range of constituent particles in $\alpha_a = [2.80, 2.88]$ and set $\alpha_c = 1.52$ (the difference in topology of these packings is shown in Fig. 2). In the packing labelled ’52’, both particles in the unit cell have a coordination number of 14 (coordination numbers were measured using the particles located in the first nearest neighbor shell), across the range of α_a studied. Similarly, in the packing labelled ’58’, both particles in the unit cell have a coordination number of 14, across the range of α_a studied. For boundary II, we set $\alpha_a = 1.80$ and studied a range of constituent particles in $\alpha_c = [1.90, 1.96]$ (the difference in topology of these packings is shown in Fig. 3). In the packing labelled ’74’, both particles in the unit cell have a coordination number of 12, across the range of α_c studied. However, in the packing labelled ’69’, both particles in the unit cell have a coordination number of 12 near $\alpha_c = 1.90$ but eventually have a coordination number of 13 near $\alpha_c = 1.96$.

We initialized systems of 1024 identical particles in both λ_A and λ_B at various densities. Particle positions and orientations were well defined for initialization in [19]. We sampled systems in the isochoric ensemble using the hard particle Monte Carlo (HPMC) [23] extension of the simulation toolkit HOOMD-blue [24, 25]. Although the volume remained fixed, box shear and aspect ratio moves were allowed, and move sizes were tuned such that acceptance ratios were approximately 0.3. We computed pressure during these simulations via the scaled distribution function [26], whose measurement is implemented in HPMC [27]. Ensemble averages were taken over five replicates and five snapshots per replicate simulation, where each simulation snapshot was separated by 10^6 MC timesteps, well beyond the calculated autocorrelation time of the system pressure. For each data point, we constructed a system in the ideal putative densest packing structure and then expanded this structure to the target packing density.

Free energies were computed via the Frenkel-Ladd [28, 29] method. The Einstein crystals for these simulations were the same packings described above, with an expansion performed down to the desired packing density at the beginning of the simulation. An external force field Λ tethered particles to their crystal sites with a spring constant of $k = \exp(25)$ in units of k_BT. We fixed length units by taking particles to have unit volume. Every 1.4×10^5 timesteps, k was linearly decreased until it was eventually 0; each time k was changed, move sizes were tuned, 10^5 timesteps were run for equilibration, and the lattice energy was computed in the remaining 4.0×10^4 timesteps.

V. RESULTS

A. Boundary I

Fig. 4(a) shows the curves of maximal packing density ϕ_d for each packing type, indicating the protected regions in darker shading under them. Below that are curves of free energy as a function of both packing and shape at various packing densities ϕ well below the maximum packing density ϕ_d. Several possibilities exist below ϕ_d, and we test for these possibilities:

- Packing states could become thermodynamically unstable at any finite packing density below ϕ_d, meaning that

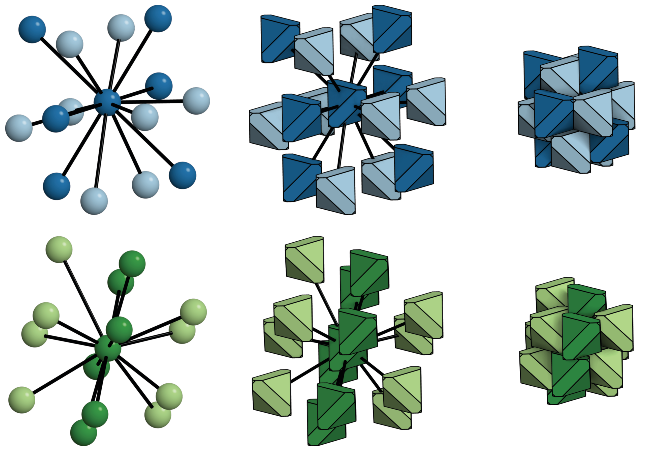

FIG. 2. Example dense packing structures (where packing $\lambda_{A=52}$ is blue and packing $\lambda_{B=58}$ is green) of anisotropic shapes, including "exploded" views that show the location and orientation of neighboring particles, and densely packed units.

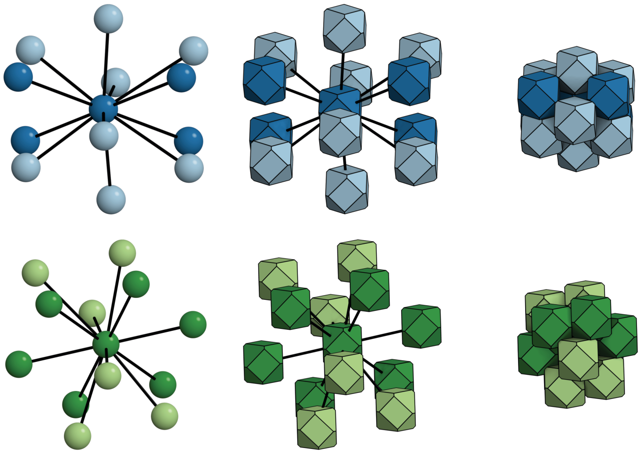

FIG. 3. Example dense packing structures (where packing $\lambda_{A=74}$ is blue and packing $\lambda_{B=69}$ is green) of anisotropic shapes, including "exploded" views that show the location and orientation of neighboring particles, and densely packed units.

packing is a kind of singular limit with no associated thermodynamic phase.

- Distinct phases persist below ϕ_d, but these phases do not preserve topological order, which would occur if other contacts proliferate in the lower packing density phases.
- Distinct phases with topological order persist.

To rule out non-existent phases, we compute the free energy of decompressed packing states. Plots of free energy (Fig. 4(a)) show that even at packing densities well below ϕ_d, two phases persist up to some crossing. The location of this crossing at packing densities below $\phi_\vee$ need not be at $\alpha_\vee$, and we find that it does deviate from $\alpha_\vee$ at lower packing density. The thermodynamically preferred regions are colored in lighter shades of the protected regions. To verify that the two phases at finite pressure have persistent and distinct topology of particle packing, we compute the relevant order parameters from Eq. (16) for each structure. This calculation is performed by extracting the unit cells of the thermalized packings of λ_A and λ_B at a packing density ϕ (the unit cell extraction technique is outlined in Appendix A).

To rule out the possibility that the phases lose topological order, we computed the θ_{ij} order parameters in the phases corresponding to thermodynamic states in our free energy calculations. We find that at packing densities well below $\phi_\vee$, phases identified by the free energy calculation correspond to phases that differ in the topology of particle contacts measured through the order parameters θ_{ij}. In Fig. 4(b,d,f) we evaluate the order parameter θ_{iA} on structures λ_i where $i \in \{A = 52, B = 58\}$ and find that over a range of packing densities, θ_{iA} evaluates to near unity on λ_A and vanishes on λ_B. Conversely, in Fig. 4(c,e,g) we evaluate the order parameter θ_{iB} on λ_A and λ_B and find that over a range of packing densities, θ_{iB} evaluates to near unity on λ_B and vanishes on λ_A.

These results indicate that the phases can be identified by the topology of the related putative densest packings, and possess residual topological order, or order that matches the order of a topological state at a packing density where topological protection has not been proven to exist. The residual topological order we observe in Fig. 4 suggests that crystal structures present in densely packed colloidal suspensions maintain a topologically consistent set of contacts between particles at densities where other competing contact topologies could exist, but are unlikely to do so due to the existence of a more thermodynamically favorable topological state.

B. Boundary II

Fig. 5(a) contains similar results for the 2nd boundary studied in this work, as it shows that a free energy crossing exists at packing densities well below the maximal packing density. In Fig. 5(b,d,f) we evaluate the order parameter θ_{iA} on structures λ_i where $i \in \{A = 74, B = 69\}$ and find that over a range of packing densities, θ_{iA} evaluates to near unity on λ_A and vanishes on λ_B. Conversely, in Fig. 5(c,e,g) we evaluate the order parameter θ_{iB} on λ_A and λ_B and find that over a range of packing densities, θ_{iB} evaluates to near unity on λ_B and vanishes on λ_A. Again, these results indicate that the phases can be identified by the topology of the related putative densest packings, and possess residual topological order. These results also suggest that this type of residual topological order can be found at valleys throughout this packing landscape, and that this type of behavior is generalizable to many different dense colloidal packings.

In this system though, it should be noted that there is noticeable deviation in the order parameters θ_{BA} and θ_{BB} as α_c approaches the value of 1.96. θ_{BA} (in Fig. 5(f)) trends slightly upward and θ_{BB} (in Fig. 5(g)) slightly downward, and it is a subtlety of the packing ($\lambda_{B=69}$) that, when captured by our order parameter, produces such deviation. We do not believe

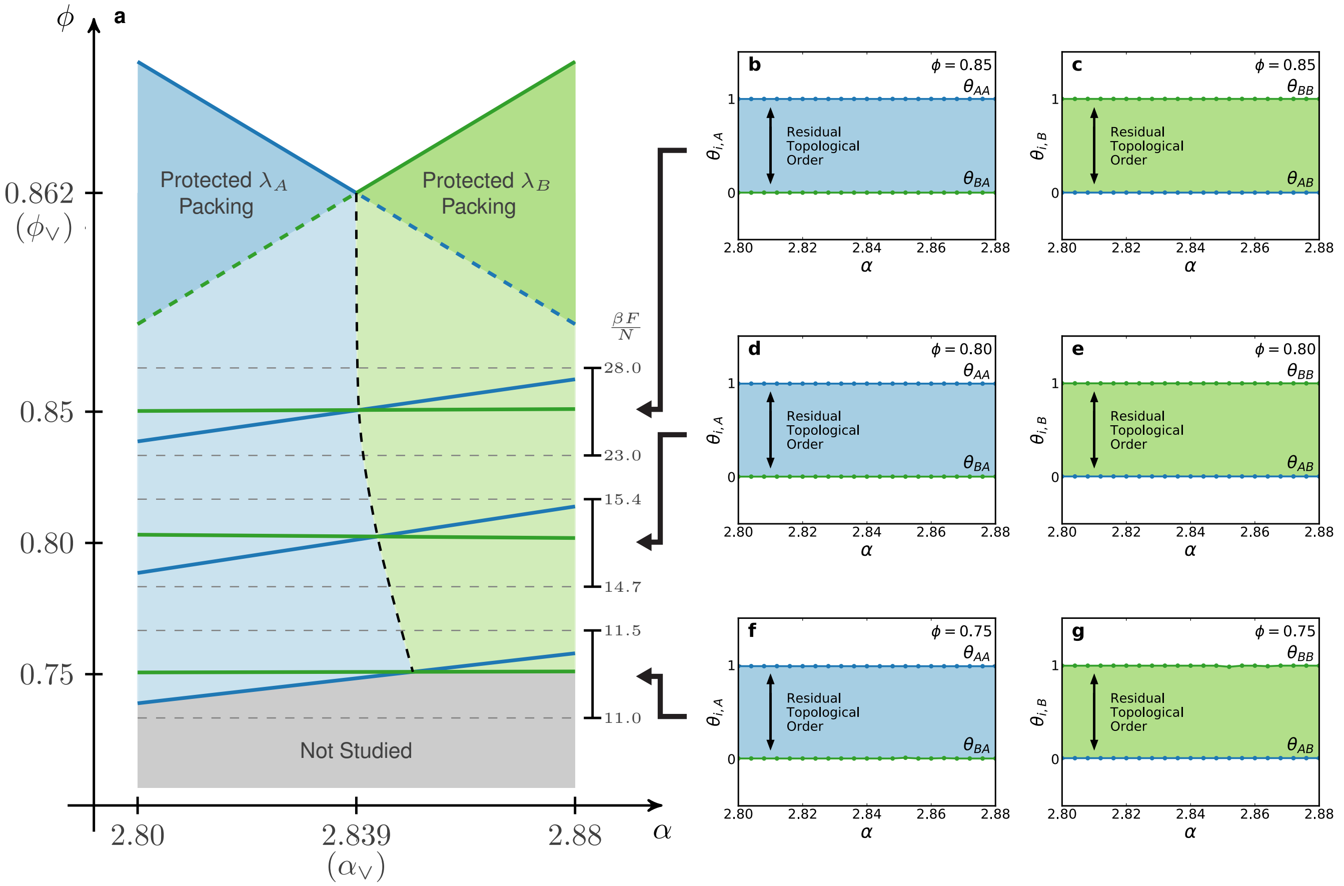

FIG. 4. Panel (a) shows the curves of maximal packing density at $\phi_\vee$, outlining the two protected packing regions, where packing $\lambda_{A=52}$ is blue and packing $\lambda_{B=58}$ is green. Lower curves indicate computed free energies at three packing densities (0.85, 0.80, 0.75). Darker shaded colors indicate protected regions, while lighter shaded colors indicate free energy preferred regions of the (α, ϕ) phase diagram. The gray region is a region where the preferred phase is unknown. Panels (b, d, f) indicate topological order evaluated using the intersection equations for $\lambda_{A=52}$ and panels (c, e, g) indicate the same using the intersection equations for $\lambda_{B=58}$. The dotted black line roughly demarcates boundaries between thermodynamically preferred packings as a function of packing density, and is meant to guide the eye.

that this slight deviation indicates a change in topology, and we address how such deviations might occur in Appendix B.

VI. DISCUSSION

The topologically distinct phases of dense suspensions of anisotropic colloids that we find here are dissimilar to topological phases in quantum matter in almost all respects, except in their stability against perturbations. For instance, whereas the topological entropy of ground-state degeneracy that arises from entanglement is important in quantum systems [30], in our systems, instead, shape entropy [2] quantifies ground state degeneracy. Moreover, whereas the geometric topology that underlies topological order in quantum systems allows a considerable mathematical apparatus to be brought to bear in understanding those states, the point-set topology that underlies the classical, topological order we identify here is more limited. Nevertheless, despite the rudimentary form of the topological order reported here, colloidal systems remain robust against perturbation, since they persist even at lower packing densities where topological protection is no longer required. This robust persistence would be a key desirable feature for applications in regimes away from the infinite pressure limit. Moreover, because the form of topological order is more rudimentary, previous work [19] demonstrating that topological features (such as particle contact types between faces, edges and vertices) generically distinguish phases of densely packed colloids suggests that this form of topological order is widespread in colloidal systems [31–35].

To leverage this topological order in experiment we note that though our order parameters are based on contact types that nominally arise at infinite pressure, we showed that topological order persists at finite pressure, meaning that alterations in contact do not proliferate at lower packing densities. This finding is potentially useful in constructing plasmonic materials that have robust response in the presence of thermal fluctuations, changes in particle shape [36] or the be-

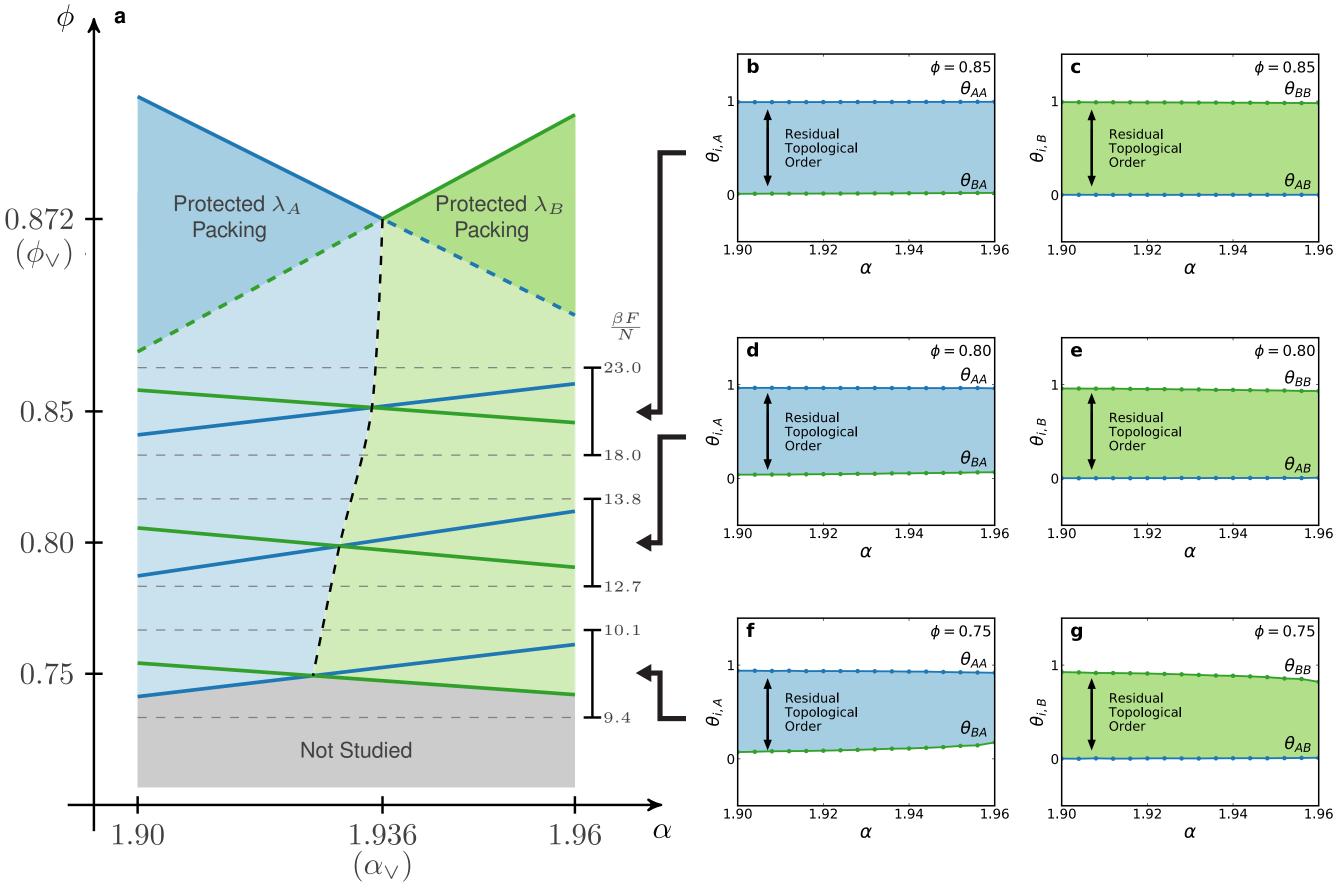

FIG. 5. Panel (a) shows the curves of maximal packing density at $\phi_\vee$, outlining the two protected packing regions, where packing $\lambda_{A=74}$ is blue and packing $\lambda_{B=69}$ is green. Lower curves indicate computed free energies at three packing densities (0.85, 0.80, 0.75). Darker shaded colors indicate protected regions, while lighter shaded colors indicate free energy preferred regions of the (α, ϕ) phase diagram. The gray region is a region where the preferred phase is unknown. Panels (b, d, f) indicate topological order evaluated using the intersection equations for $\lambda_{A=74}$ and panels (c, e, g) indicate the same using the intersection equations for $\lambda_{B=69}$. The dotted black line roughly demarcates boundaries between thermodynamically preferred packings as a function of packing density, and is meant to guide the eye.

havior of stabilizing ligands [37, 38]. It is known that the plasmonic response of systems of anisotropic nanoparticles depends strongly on the type of contacts between nanoparticles [39]. We find that the topology of contacts between anisotropic nanoparticles is stable over a broad range of packing densities. When situated in the context of the zoo of distinct sets of contact types that has been shown to exist [19] in families of anisotropic nanoparticles and the variety of synthesis techniques that can readily produce such particles in the laboratory [40–43], our work points to potential avenues for creating nanomaterials with a diversity of robust forms of plasmonic response.

VII. ACKNOWLEDGMENTS

Research for this publication was conducted with Government support under contract FA9550-11-C-0028 and awarded by the Department of Defense, Air Force Office of Scientific Research, National Defense Science and Engineering Graduate (NDSEG) Fellowship, 32 CFR 168a, awarded to W.E.Z. E.G.T acknowledges support from the National Science Foundation Graduate Research Fellowship Grant DGE 1256260 and a Blue Waters Graduate Fellowship. This research is part of the Blue Waters sustained petascale computing project, which is supported by the National Science Foundation (awards OCI-0725070 and ACI-1238993) and the state of Illinois. Blue Waters is a joint effort of the University of Illinois at Urbana-Champaign and its National Center for Supercomputing Applications. This work was partially supported by a Simons Investigator award from the Simons Foundation to Sharon Glotzer. Computational resources and services supported by Advanced Research Computing at the University of Michigan, Ann Arbor. We thank D. Klotsa and E. R. Chen for access to data pertinent to this study and helpful discussion of that data. We also thank J. Dshemuchadse and B. VanSaders for helpful discussions and software contributions.

Appendix A: Unit Cell Extraction

To perform the order parameter calculation described in the main text, one must compute a set of intersection expressions of the form

$$C_{\lambda,k}(\alpha_a, \alpha_c, \vec{a}, \vec{b}, \vec{c}, \vec{d}) \tag{A1}$$

where λ is a lattice, α_a and α_c are shape parameters of the particle, $\{\vec{a}, \vec{b}, \vec{c}\}$ are the lattice vectors of the two particle unit cell, and $\vec{d}$ is the displacement vector between the particles in the two-particle unit cell. While the shape parameters are readily available during the calculation of these intersection equations, unit cell information is not. We extracted this information from each thermalized system snapshot in the following manner:

1. We extracted the lattice vectors $\{\vec{a}, \vec{b}, \vec{c}\}$ from the snapshot.
2. We used the unit cell defined by the extracted lattice vectors to find the lattice basis.
3. We iterated through all possible (right-handed) permutations of the lattice vectors, and associated transformations of the basis such that it remained in the interior of the unit cell, to minimize $\sum_{k=1}^{K_\lambda} \left|C_{\lambda,k}\right|$, defined in the main text.

To extract the lattice vectors, we first chose a subset of particles, hereafter called $\{O\}$, that we initialized to have identical locations in the unit cell of the lattice. We calculated the local environment of each member i of $\{O\}$, defined as the set of its J nearest neighbor vectors $\vec{r}_{ij} = \vec{r}_j - \vec{r}_i$, where j is an index over the J nearest neighbors of i that are also members of $\{O\}$. We then clustered members of $\{O\}$ by the similarity of their environment according to an "environment matching" scheme, which we have made available as a part of the open-source analysis package *freud* [44]. Briefly, the software determines if a set of N vectors $\{\vec{r}\}$ is similar to, or "matches," another set of N vectors $\{\vec{r'}\}$, by attempting to find a one-to-one mapping between $\{\vec{r}\}$ and $\{\vec{r'}\}$ such that $|\vec{r}_n - \vec{r'}_{n'}| < t$ for every mapping pair (n, n') for some threshold t. $\vec{r}_n$ is the n-th member of $\{\vec{r}\}$, and $1 \leq n \leq N$. $\vec{r'}_{n'}$ is the n'-th member of $\{\vec{r'}\}$, and $1 \leq n' \leq N$. If that mapping is found, then $\{\vec{r}\}$ and $\{\vec{r'}\}$ "match." Here, we compared the environment of every member of $\{O\}$ to every other member of $\{O\}$. We chose J by inspection, to produce an environment for each member of $\{O\}$ that would be approximately similar to eye and that would contain vectors capable of spanning three dimensions. We chose $t = 0.1\langle r_{max}\rangle$, where $\langle r_{max}\rangle$ is the average over the set of distances from every member of $\{O\}$ to its J-th nearest neighbor (also in $\{O\}$).

We chose the largest subset of members of $\{O\}$ with matching environments, $\{O_m\}$, and took the average environment over the set of environments of all members of $\{O_m\}$. We then found a minimal volume unit cell from these J average vectors. We computed the Niggli reduced cell [45] from this minimal volume unit cell using the open-source software package *niggli*, available at `https://github.com/atztogo/niggli`.

We then extracted the unit cell basis. To do this, we constructed a new local environment for every member i of $\{O\}$, this time consisting of K nearest neighbor vectors $\vec{r}_{ik} = \vec{r}_k - \vec{r}_i$, where k is an index over the K nearest neighbors of i, regardless of whether those neighbors are members of $\{O\}$ or not. We computed the average local environment over every environment found in this manner, and wrapped these average neighbor vectors into the reduced unit cell found in the previous step. We clustered the wrapped neighbor locations using the DBSCAN clustering algorithm [46] in the *scikit-learn* Python module [47], and determined average positions of all clusters of points. We verified that our clustering procedure produced two positions in the unit cell, one near a unit cell corner and one in the interior of the unit cell. We determined K by automatically detecting a minimal cut-off radius r_{cut} within which all particles had a number of nearest neighbors in a small, two-member set of nearest neighbor numbers $\{K'\}$. We imposed an additional constraint that both members of $\{K'\}$ had to be greater than 10, in order to find suitable environments for basis extraction. We then chose K to be the larger member of $\{K'\}$ that resulted in a clean, two-particle basis by the method above.

We then took a corner of the unit cell to be the origin of our coordinate system, and defined the displacement vector $\vec{d}$ to point from this origin to the basis position in the interior of the cell. Each possible corner-origin corresponded to a triplet of permutations of lattice vectors such that they remained right-handed. We iterated through all corners and associated triplets to minimize $\sum_{k=1}^{K_\lambda} \left|C_{\lambda,k}\right|$, defined in the main text. Additional special care had to be taken to compare our extracted unit cells with the unit cells as expressed in Ref. [19]; those minutiae were specific to the way we initialized our simulations and will not be discussed here.

Appendix B: Effectiveness of the Order Parameter

The order parameter, as previously described, uses the unit cell geometry in order to characterize the topology of a packing. Specifically, we extract unit cell parameters (described above) and evaluate the appropriate, unique, intersection inequalities in order to describe the topology of the packing. When a packing is no longer maximally dense ($\phi < \phi_d$), the inequalities are no longer saturated (by definition) and θ_{ij} can, and in general will, be less than one. However, there are different ways that a packing can expand. It could expand in a direction where space emerges more quickly between contacts shared with the adjacent packing (which would not be reflected in θ_{ij}) or could change more quickly for contacts that appear in one packing and not in the other (which would result in a change in θ_{ij}). Therefore, the fact that we observe small deviations in θ_{ij} is not surprising and expected.

As an example, consider the packing $\lambda_{B=69}$ as seen in Fig. 5, specifically the order parameter where this packing is eval-

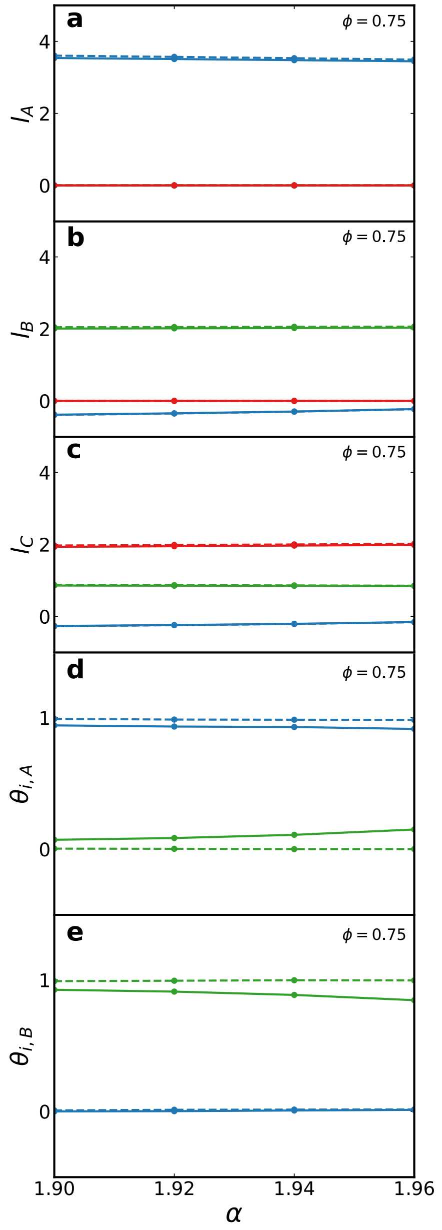

FIG. 6. Panel (a) shows the vector components (a_x (blue), a_y (green), a_z (red)) for the simulation box (dashed) and the extracted unit cell (solid) of $\lambda_{B=69}$. The box vectors are scaled uniformly to match the unit cell vectors. In panel (a), the a_y and a_z fall directly onto one another, so both cannot be seen. Panels (b) and (c) show the same but instead for (b_x, b_y, b_z) and (c_x, c_y, c_z) respectively. Panel (d) shows the comparison of the order parameters θ_{AA} (blue) and θ_{BA} (green) for both the system with box moves (solid) and without box moves (dashed). Panel (e) shows the same but for θ_{AB} (blue) and θ_{BB} (green).

uated in its own intersection equations (θ_{BB}). At $\phi = 0.85$, we can see that θ_{BB} remains around unity (Fig. 5(c)) as we move along $\alpha_c = [1.90, 1.96]$ and that θ_{BB} behaves similarly for $\phi = 0.80$ (Fig. 5(e)), although this time it remains slightly below unity. However, at $\phi = 0.75$ (Fig. 5(g)), θ_{BB} decays slightly as we approach $\alpha_c = 1.96$, away from unity. Additionally, we see that when this packing is evaluated in the other packing's intersection equations (Fig. 5(f)), that θ_{BA} increases slightly as we approach $\alpha_c = 1.96$, away from zero.

This would seem to imply that the topology appreciably changes as we move toward $\alpha_c = 1.96$, but visual inspection confirms that this is not the case. We instead postulate that each packing type λ_i (where $i \in \{A, B\}$) has a unique response to collective motion in the system, where collective motion comes from Monte Carlo box moves used in our simulations, which involve box aspect ratio moves (which attempt to change the box aspect ratio) and box shear moves (which attempt to shear the box). Since each packing is defined in a different way, each packing could have a unique response to this collective motion and therefore cause one of the scenarios for contacts described above.

We studied the packing $\lambda_{B=69}$ in order to prove that collective motion is the cause of changes in θ_{BB} and θ_{BA} at $\phi = 0.75$. First, we performed NPT simulations of $\lambda_{B=69}$ with Monte Carlo box moves turned on, for four statepoints ($\alpha_c = [1.90, 1.92, 1.94, 1.96]$), so that we could better examine the effect of box moves as a function of shape. The system box vector components (which are scaled by a constant factor representing the box-to-unit-cell size ratio) are plotted (dashed lines) along with extracted unit cell vectors (solid lines) in Fig. 6(a,b,c). Each point represents the vector component averaged over five frames of a simulation (where each frame is separated by 10^6 MC timesteps). As we move from $\alpha_c = 1.90$ to $\alpha_c = 1.96$, we show both sets of vectors to confirm two things: (i) our extracted unit cell vectors match the box vectors when appropriately scaled and (ii) as the shape parameter changes from $\alpha_c = 1.90$ to $\alpha_c = 1.96$, there is an appreciative change in several of the vector components, enough that we believe this would significantly change the value of the order parameter, since it is a function of extracted unit cell parameters. In $\lambda_{B=69}$ the unit cell naturally lengthens as a function of the shape parameter, which can be seen in [19]. It appears that because of this fact, more box moves are accepted that result in a change in the x-components of all three lattice vectors (shown in blue in Fig. 6(a,b,c)), allowing for the box to lengthen further as we move from $\alpha_c = 1.90$ to $\alpha_c = 1.96$.

Next, we show what happens if Monte Carlo box moves are removed from the simulation and the only moves that are allowed are typical translation/rotation moves. We took the same four shape parameters $\alpha_c = [1.90, 1.92, 1.94, 1.96]$ and this time performed two simulations for each shape, one where these box moves were applied and one where they were not. Results of these simulations are included in Fig. 6(d,e). Each point represents the average order parameter over five frames of a simulation where each frame is separated by 10^6 MC timesteps. The points connected by a solid line represent simulations where box moves are turned on (similar to the order parameters shown in Fig. 5(f,g)) and the dashed lines where box moves are turned off. From the figure it is clear that box moves are driving the order parameters away from zero in the case of θ_{BA} and from unity in the case of θ_{BB}.

We believe that this actually further emphasizes the topological order exhibited by these dense packings, since even when collective motion is allowed to occur in the system, it only seems to change the calculated order parameters by a small amount at $\phi = 0.75$ as seen in Fig. 5, and visual inspection confirms that the topological character of the packings remains the same.

[1] E. Dennis, A. Kitaev, A. Landahl, and J. Preskill, J. Math. Phys. **43**, 4452 (2002).

[2] G. van Anders, D. Klotsa, N. K. Ahmed, M. Engel, and S. C. Glotzer, Proc. Natl. Acad. Sci. U.S.A. **111**, E4812 (2014), arXiv:1309.1187 [cond-mat.soft].

[3] D. Frenkel, Nat. Mater. **14**, 9 (2015).

[4] D. Klotsa, E. R. Chen, M. Engel, and S. C. Glotzer, Soft Matter (2018), 10.1039/c8sm01573b.

[5] Y. Zhang, F. Lu, D. van der Lelie, and O. Gang, Phys. Rev. Lett. **107**, 135701 (2011).

[6] O. Gang and Y. Zhang, ACS Nano **5**, 8459 (2011).

[7] Y. Peng, F. Wang, Z. Wang, A. M. Alsayed, Z. Zhang, A. G. Yodh, and Y. Han, Nat Mater **14**, 101 (2015).

[8] C. X. Du, G. van Anders, R. S. Newman, and S. C. Glotzer, Proc. Natl. Acad. Sci. U.S.A. **114**, E3892 (2017), arXiv:1603.00727 [cond-mat.soft].

[9] C. Kane and T. Lubensky, Nature Physics **10**, 39 (2014).

[10] J. Loehr, M. Loenne, A. Ernst, D. de Las Heras, and T. M. Fischer, Nature Communications **7**, 11745 (2016).

[11] J. Loehr, D. de las Heras, A. Jarosz, M. Urbaniak, F. Stobiecki, A. Tomita, R. Huhnstock, I. Koch, A. Ehresmann, D. Holzinger, and T. M. Fischer, Communications Physics **1**, 4 (2018).

[12] E. Prodan and C. Prodan, Physical Review Letters **103**, 248101 (2009).

[13] S. H. Mousavi, A. B. Khanikaev, and Z. Wang, Nature Communications **6**, 8682 (2015).

[14] P. Wang, L. Lu, and K. Bertoldi, Physical Review Letters **115**, 104302 (2015).

[15] C. He, X. Ni, H. Ge, X.-C. Sun, Y.-B. Chen, M.-H. Lu, X.-P. Liu, and Y.-F. Chen, Nature physics **12**, 1124 (2016).

[16] E. Prodan, K. Dobiszewski, A. Kanwal, J. Palmieri, and C. Prodan, Nature Communications **8**, 14587 (2017).

[17] J.-W. Jiang and H. S. Park, Journal of applied physics **125**, 082511 (2019).

[18] L. Lu, J. D. Joannopoulos, and M. SoljaÄ■iÄĞ, Nature photonics **8**, 821 (2014).

[19] E. R. Chen, D. Klotsa, M. Engel, P. F. Damasceno, and S. C. Glotzer, Phys. Rev. X **4**, 011024 (2014), arXiv:1309.2662 [cond-mat.soft].

[20] G. van Anders, D. Klotsa, A. S. Karas, P. M. Dodd, and S. C. Glotzer, ACS Nano **9**, 9542 (2015), arXiv:1507.04960 [cond-mat.soft].

[21] Strictly, $\tilde{F}$ should be evaluated at $\phi_d(\alpha_\vee^-), \alpha_\vee^-$ because the free energy of the packing at $\alpha_\vee^+$ might be different; we use $\tilde{F}(\phi_\vee, \alpha_\vee)$ for convenience.

[22] Note that if subsequent evaluation of the order parameter indicates the state is not isostructural with λ_i it implies those structures are thermodynamically unstable.

[23] J. A. Anderson, M. Eric Irrgang, and S. C. Glotzer, Comput. Phys. Commun. **204**, 21 (2015).

[24] J. A. Anderson and S. C. Glotzer, (2013), `http://codeblue.umich.edu/hoomd-blue`, arXiv:1308.5587 [physics.comp-ph].

[25] J. Glaser, T. D. Nguyen, J. A. Anderson, P. Lui, F. Spiga, J. A. Millan, D. C. Morse, and S. C. Glotzer, Comput. Phys. Commun. **192**, 97 (2015).

[26] M. Engel, J. A. Anderson, S. C. Glotzer, M. Isobe, E. P. Bernard, and W. Krauth, Phys. Rev. E **87**, 042134 (2013).

[27] J. A. Anderson, M. E. Irrgang, and S. C. Glotzer, Comp. Phys. Commun. **204**, 21 (2016).

[28] D. Frenkel, J. Chem. Phys. **81**, 3188 (1984).

[29] A. Haji-Akbari, M. Engel, and S. C. Glotzer, J. Chem. Phys. **135**, 194101 (2011), arXiv:1106.4765 [cond-mat.soft].

[30] A. Kitaev and J. Preskill, Phys. Rev. Lett. **96**, 110404 (2006).

[31] J. de Graaf, R. van Roij, and M. Dijkstra, Phys. Rev. Lett. **107**, 155501 (2011), arXiv:1107.0603 [cond-mat.soft].

[32] U. Agarwal and F. A. Escobedo, Nat. Mater. **10**, 230 (2011).

[33] R. Ni, A. P. Gantapara, J. de Graaf, R. van Roij, and M. Dijkstra, Soft Matter **8**, 8826 (2012), arXiv:1111.4357 [cond-mat.soft].

[34] P. F. Damasceno, M. Engel, and S. C. Glotzer, ACS Nano **6**, 609 (2012), arXiv:1109.1323 [cond-mat.soft].

[35] A. P. Gantapara, J. De Graaf, R. Van Roij, and M. Dijkstra, Physical Review Letters **111**, 1 (2013).

[36] G. van Anders, N. K. Ahmed, R. Smith, M. Engel, and S. C. Glotzer, ACS Nano **8**, 931 (2014), arXiv:1304.7545 [cond-mat.soft].

[37] C. Waltmann, N. Horst, and A. Travesset, ACS Nano **11**, 11273 (2017).

[38] T. Waltmann, C. Waltmann, N. Horst, and A. Travesset, Journal of the American Chemical Society **140**, 8236 (2018).

[39] A. Tao, P. Sinsermsuksakul, and P. Yang, Nat. Nanotechnol. **2**, 435 (2007).

[40] Y. Xia, Y. Xiong, B. Lim, and S. Skrabalak, Angew. Chem., Int. Ed. **48**, 60 (2009).

[41] J. Henzie, M. Grünwald, A. Widmer-Cooper, P. L. Geissler, and P. Yang, Nat. Mater. **11**, 131 (2012).

[42] M. H. Huang and P.-H. Lin, Advanced Functional Materials **22**, 14 (2012).

[43] C.-W. Liao, Y.-S. Lin, K. Chanda, Y.-F. Song, and M. H. Huang, Journal of the American Chemical Society **135**, 2684 (2013).

[44] V. Ramasubramani, B. D. Dice, E. S. Harper, M. P. Spellings, J. A. Anderson, and S. C. Glotzer, arXiv preprint arXiv:1906.06317 (2019).

[45] P. Niggli, *Krystallographische und Strukturtheoretische Grundbegriffe*, Vol. 7 (Akademische Verlagsgesellschaft, Leipzig, Germany, 1928).

[46] M. Ester, H. Kriegel, J. Sander, and X. Xu, in *Proceedings of the 2nd International Conference on Knowledge Discovery and Data Mining* (AAAI Press, Portland, OR, 1996) pp. 226–231.

[47] F. Pedregosa, G. Varoquaux, A. Gramfort, V. Michel, B. Thirion, O. Grisel, M. Blondel, P. Prettenhofer, R. Weiss, V. Dubourg, J. Vanderplas, A. Passos, D. Cournapeau, M. Brucher, M. Perrot, and E. Duchesnay, Journal of Machine Learning Research **12**, 2825 (2011).